Non-contact Optical Respiratory Rate and Heart Rate Monitoring Sensor based on the Six-Hole High Birefringence Fiber

Yujian Li, Pin Xu, Zhengyong Liu, Weimin Lyu, and Changyuan Yu, *Senior Member, IEEE*

***Abstract*—In this paper, an optical respiratory and heart rate non-invasive monitoring sensor is set up and proven to work well. The core part of this sensor is an optical fiber Sagnac interferometer (SI), built up by a 3 dB coupler and a section of homemade Six Holes High Birefringence Fiber (SH-HiBiF). Because of the circular asymmetric structure in the fiber, the wavelength-domain spectroscopy of the SI will shift linearly with the lateral stress changes with a sensitivity of 1.72 nm/kPa. Thus, if a single-wavelength laser is injected into the fiber, the respiratory and heart rate signals can modulate the light intensity and finally be demodulated by a photoelectric detector (PD). The heartbeat signals acquired by the proposed sensor demonstrate a high consistency (up to 95%) with those obtained from conventional electrical sensors, as validated by Bland-Altman analysis. Furthermore, the proposed monitoring sensor can help confirm the diagnosis of premature atrial contraction (PAC) even if it is not in contact with the human body, which is more comfortable for the patients. The temperature cross-sensitivity of this monitoring sensor is relatively low because the raw material of the sensing part is pure fused silica. Performed experiments demonstrate the sensor's feasibility in further research in the biomedical field.**

***Index Terms*—birefringence fiber, cardiac premature beat, heart rate, non-invasive, respiratory rate, Sagnac interference.**

I. INTRODUCTION

THE variation of respiratory rate (RR) and heart rate (HR) is an important early warning signal of many diseases, such as cardiovascular diseases [1], fatigue [2], apnea [3], mental stress [4], and respiratory abnormalities [5]. Continuous monitoring of RR and HR for the patients allows medical workers to evaluate the patient's physiological condition timely manner and then implement intervention therapy appropriately.

In recent years, various electrical sensors based on different data acquisition methods have been proposed for HR monitoring, such as a fingertip cardio tachometer [6], wrist cardio tachometer [7], and chest electrodes electrocardiogram instrument [8]. As for RR monitoring, the head-mounted respiratory monitor takes up the primary market [9]. However, all electrical sensors cannot be used in high electromagnetic environments, such as magnetic resonance imaging equipment, because they are susceptible to electromagnetic interference. Moreover, most electrical sensors are direct contact type, which is uncomfortable with constraints on the person's activities.

Using indirect contact optical fiber sensors as the main sensing element in the vital signs monitoring system is an ingenious way to solve electromagnetic interference and comfort problems [10]. In addition, optical fiber sensors possess many unique advantages, such as compact size [11], lightweight, chemical corrosion resistance [12], and long-term stability. An increasing number of optical fiber sensor-based monitoring sensors proposed by researchers worldwide also prove the advantages. In 2014, Chen et al. used a micro-bend multimode fiber sensor to simultaneously measure the HR and RR [13]. In 2016, Massaroni et al. designed a smart textile based on fiber Bragg grating (FBG) for RR monitoring [14]. In 2019, Tan et al. proposed a twin-core fiber (TCF)-based sensor for non-invasive RR and HR monitoring. In 2021, Yuan et al. successfully fabricated an all-fiber sensor based on the hollow core Bragg fiber (HCBF) and used it to monitor human breath [16]. However, the limitation of the above sensors is that they are temperature sensitive, which requires recalibration under different temperature conditions.

This paper proposes a temperature-insensitive sensor based on an optical fiber sensor for non-contact vital signs monitoring. The core sensing element is a Sagnac Interferometer (SI) built up by an optical coupler and a six-hole high birefringence fiber (SH-HiBiF). The SH-HiBiF is a type of temperature-insensitive fiber because its raw material is pure fused silica without doping other particles. Due to the stress-induced birefringence effect in this fiber, the interference spectrum of the SI connected with a broadband light source will experience linear shifts with variations in lateral stress.

Manuscript received XXXX; revised XXXX; accepted XXXX. Date of publication XXXX; date of current version XXXX. This work was supported by Ultrafast and ultrahigh-resolution optical spectrum response measurement based on linear frequency modulation (HK RGC GRF 15209321 B-Q85G) and Non-wearable non-invasive photonic smart health monitoring system for atrial fibrillation diagnosis based on optical fiber sensor with machine learning (HKPU 1-CD8N) (Corresponding author: Weimin Lyu).

Yujian Li, Pin Xu, and Weimin Lyu are with Photonics Research institute, the Department of Electrical and Electronic Engineering, The Hong Kong Polytechnic University, Hong Kong 999077, China.

Zhengyong Liu is with Guangdong Provincial Key Laboratory of Optoelectronic Information Processing Chips and sensors, School of Electronics and Information Technology, Sun Yat-sen University, Guangzhou 510275, China, and also is with Southern Marine Science and Engineering Guangdong Laboratory (Zhuhai), Zhuhai 519000, China.

Changyuan Yu is with Photonics Research Institute, the Department of Electrical and Electronic Engineering, The Hong Kong Polytechnic University, Hong Kong 999077, China, and is also with Shenzhen Research Institute, The Hong Kong Polytechnic University, Shenzhen, China.

Color versions of one or more of the figures in this article are available online at http://ieeexplore.ieee.org

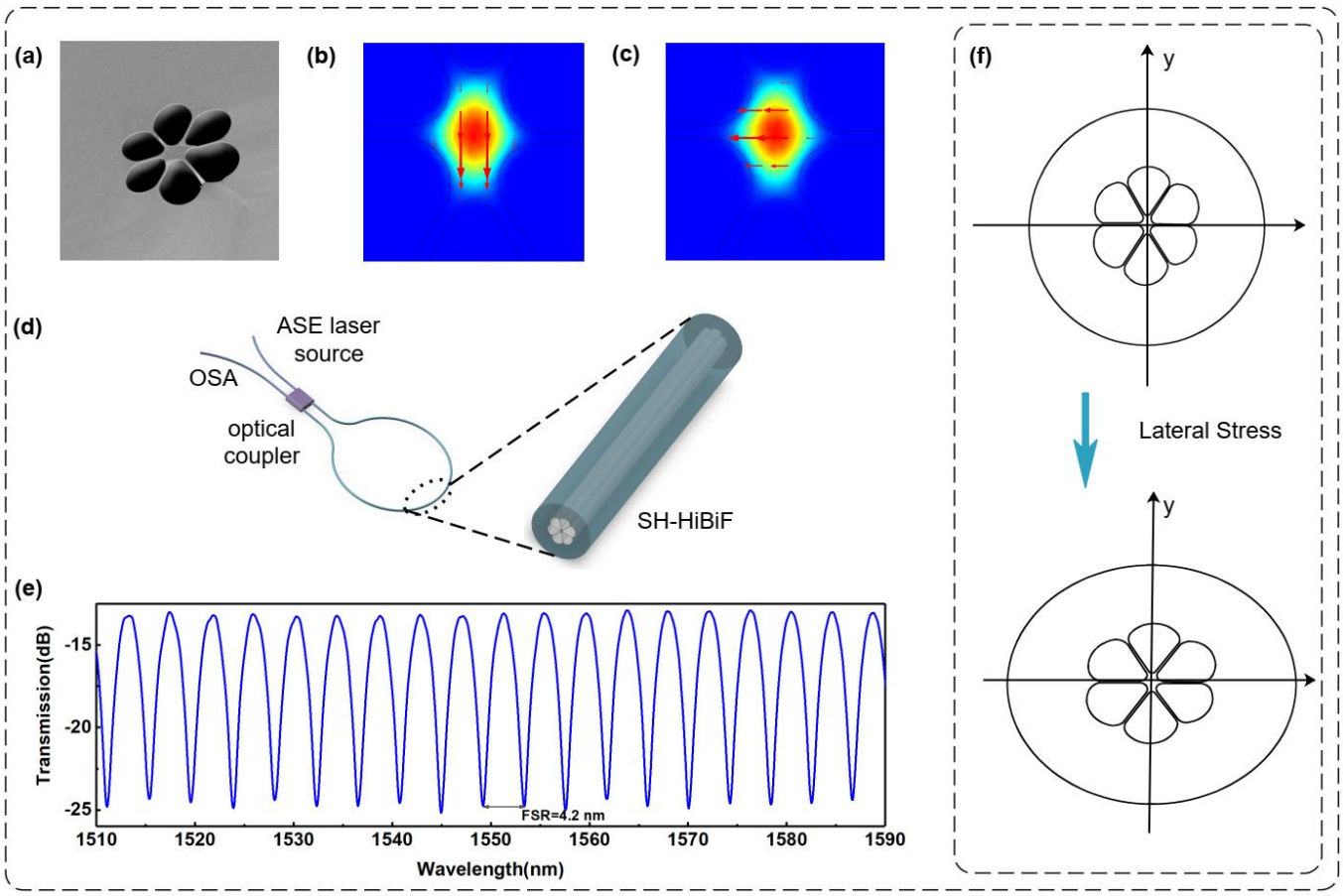

Fig. 1. (a) The cross-section of the SH-HiBiF under the SEM; (b) the simulation mode field distribution of LP_{01}-y; (c) the simulation mode field distribution of LP_{01}-x; (d) the structure of the SI based on SH-HiBiF; (e) the transmission spectrum of the SI under broadband spectrum light source, of which the free space range (FSR) is 4.2 nm; (f) the structural sketch of the cross-section change result of the SH-HiBiF from zero external force to under lateral stress.

The wavelength shift can be converted into the light intensity change by changing the light source from a broadband to a single-wavelength laser source around the Q points (the points on the interference spectrum with the highest slope). As a result, the output light intensity will be modulated by the HR and RR signals. Then, demodulating by a photodetector (PD), the output light intensity signal with HR and RR signals can be converted into an electronic signal. Subsequent data processing facilitates the extraction of the individual's HR and RR signals.

During the experiment process, this sensor operates reliably with people of different genders and ages. In addition, the designed sensor can easily distinguish whether someone has the symptom of Premature Atrial Contraction (PAC) even without having any contact with the person's body. This sensor is a better choice for patients who need vital signs monitoring free from electromagnetic interference or a more comfortable monitoring experience.

II. Sagnac Interferometer

A. Six-Hole High Birefringence Fiber

The cross-section of the fiber used for building up the SI is displayed in Fig. 1(a). Same as the standard single-mode fiber (SMF), the outer diameter of the fiber is 125 μm. Six drop-shaped air holes distributed evenly surround the central point of the fiber. The dimension of each hole is ~22 μm×~ 27 μm. Because of the circular asymmetric structure of the suspended core part, a stress-induced birefringent effect is introduced into this fiber. The size of the central suspension part is ~8 μm×4 μm.

The simulation results of the fundamental core mode are shown in Fig. 1 (b) and (c). The red arrows point in the direction of the electric fields. The calculated fundamental mode is elliptical, with two perpendicular polarization states LP_{01}-x and LP_{01}-y. The ERI of them is 1.43546, and 1.43572 @ 1550 nm, giving a phase modal birefringence B of ~ 2.6×10^{-4} @1550 nm. Thus, this fiber can be used for building up SI with an optical coupler as shown in Fig. 1(d). The transmitted spectrum with 105 cm SH-HiBiF is shown in Fig. 1(e). The spectrum's waveform is a typical interference waveform. The free spectrum range of it around 1550 nm is about 4.2 nm.

B. Spectrum Analysis and Sensing Principle

Suppose the light intensity of the two perpendicular polarization states is I_1 and I_2. In that case, the wavelength is λ, the ERI are n1 and n2, and the fiber length is L; the output light intensity of the proposed SI under a broadband light source is expressed as:

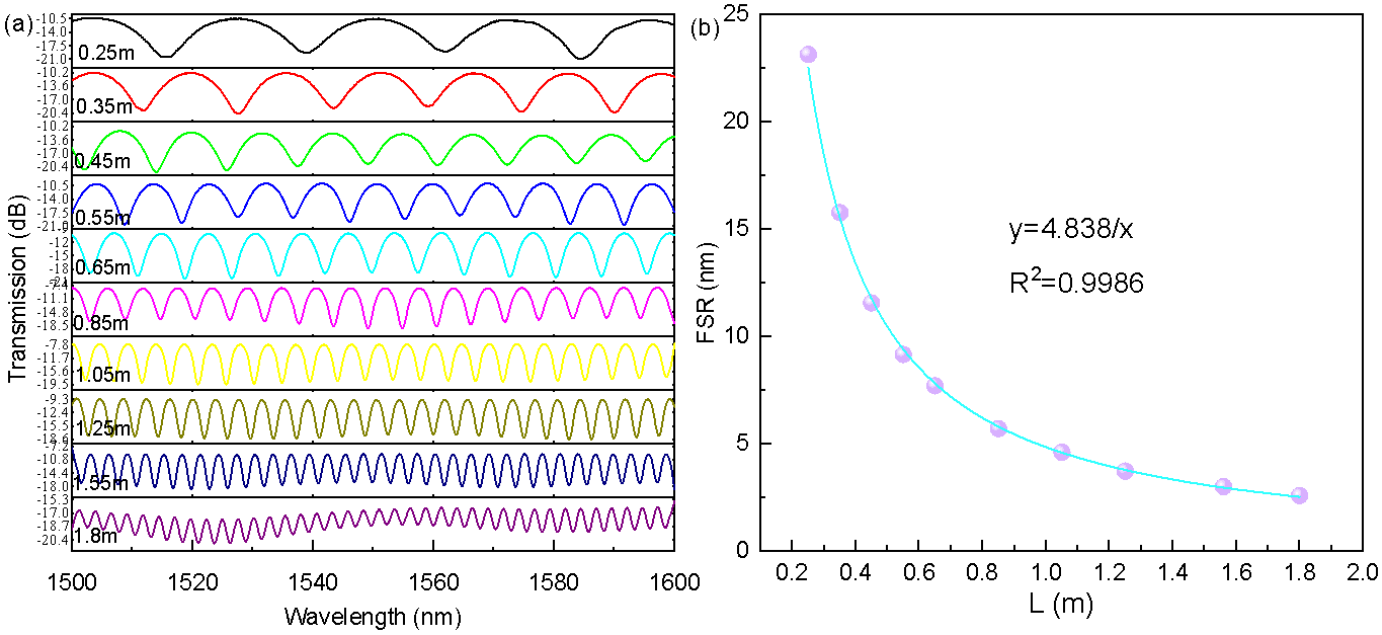

Fig. 2. (a) Transmission spectrum of SI with different SH-HiBiF lengths; (b) Fitting relationship between FSR and SH-HiBiF length.

$$I(\lambda) = I_1 + I_2 + 2\sqrt{I_1 I_2}\cos\left[\frac{2\pi}{\lambda}B(\lambda)L\right]. \quad (1)$$

When the phase φ equals $2(m+1)\pi$, the intensity of the output light will reach the minimum value. The wavelength difference between two adjacent minima is referred to as FSR, which can be expressed as:

$$\frac{d\varphi}{d\lambda}\bullet FSR = 2\pi. \quad (2)$$

A more specific form of (2) is:

$$\left[\frac{2\pi L}{\lambda}\frac{dB(\lambda)}{d\lambda} - \frac{2\pi LB(\lambda)}{\lambda^2}\right]FSR = 2\pi. \quad (3)$$

Then FSR around 1550nm can be calculated as:

$$FSR_{1550nm} = \frac{\lambda^2}{\left[\lambda\frac{dB(\lambda)}{d\lambda} - B(\lambda)\right]L} = \frac{5.0579}{L}. \quad (4)$$

The units of L and FSR are meter and nanometer, respectively. To verify the correctness of the derivation results, a series of SIs under different SH-HiBiF lengths are fabricated and their transmission spectrum are shown in Fig. 2(a). The FSR decreases as the fiber length increases. The fitting relationship between FSR and L is shown in Fig. 2(b), which is inversely proportional. The fitting parameter is 4.838, which is quite close to 5.0579 in Eq. (4). The difference between theoretical and factual values results from the measurement error of fiber length and the approximate computing error.

The external lateral stress change can be measured by the SI loop because of the elastic-optical effect. As shown in Fig. 1(f), the fiber will deform, and then the ERI of the two perpendicular polarization lights changes correspondingly. If choosing a specific interference dip as the monitoring dip and ignoring the length variation caused by lateral stress, the relationship between wavelength shift and lateral stress can be calculated as:

$$\frac{d\lambda}{dP} = \frac{2L}{2m+1}\frac{dB(\lambda)}{dP}. \quad (5)$$

III. Lateral Stress Sensing

The emitted light originates from an Amplified Spontaneous Emission (ASE) laser, spanning a spectral range from 1500 nm to 1600 nm. Subsequently, the final spectrum is captured utilizing an Optical Spectrum Analyzer (OSA, AQ6070D), of which the resolution is 0.02 nm. To facilitate measurement, approximately 80 cm of SH-HiBiF is coiled and secured to a horizontal platform. Another acrylic plate is then positioned atop the fiber to ensure uniform pressure distribution as shown in Fig. 3(a). The SH-HiBiF section in the SI ring is put between the plates, while the SMF section is put outside the plate to make sure the lateral stress is exclusively applied to the SH-HiBiF. The pressure exerted by weights induces this lateral stress variance, each measuring 1.25 kg. With the dimensions of the acrylic plate at 20 cm × 10 cm, the pressure intensity exerted on the fiber by each weight is calculated to be 625 Pa.

The interference dip shifts with variations in lateral stress, as depicted in Fig. 3(c). Notably, the spectrum shifts towards shorter wavelengths with increasing lateral stress. Fig. 3(b) displays the linear relationship between pressure intensity and dip wavelength around 1550 nm. The slope of the fitting curve signifies the sensitivity, computed as 1.72 pm/Pa (equivalent to 1.72 nm/kPa). The substantial degree of fitting, with an R^2 value of 0.99043, suggests that the sensor demonstrates a linear response to alterations in lateral stress.

Furthermore, the sensor exhibits minimal sensitivity to temperature fluctuations owing to the fabrication material of the SH-HiBiF, which consists of pure fused silica without any doped particles [17]. Consequently, temperature variations do not affect the characteristics of the sensor, rendering it more stable for practical applications.

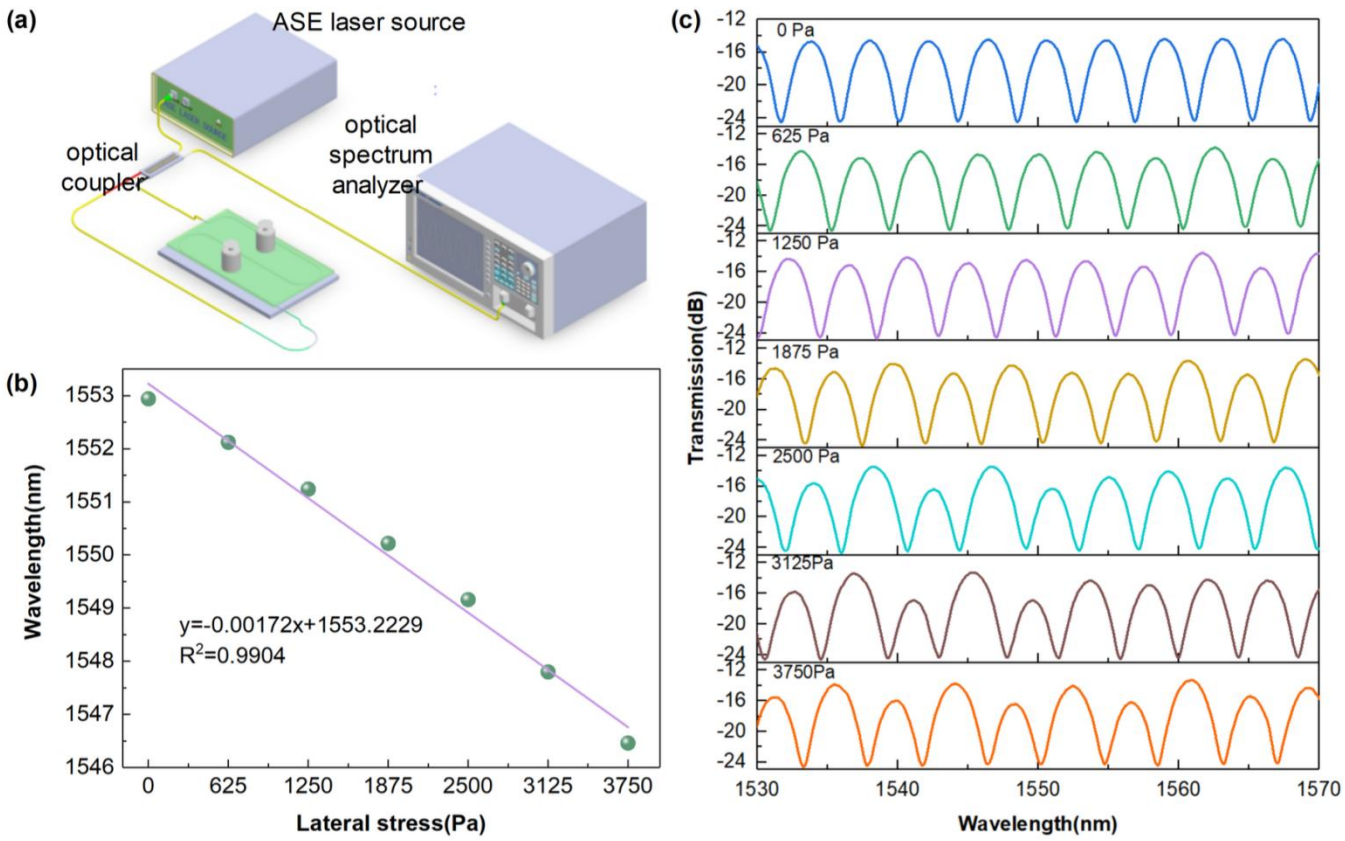

Fig. 3. (a) The experiment sensor for the lateral stress sensing; (b) The fitting curve between the interference dip around 1550 nm and added lateral stress; (c) The sensor spectrum under different lateral stress.

IV. Vital Signs Monitoring

From the experiment results mentioned above, it's evident that the designed SI effectively detects lateral stress changes by monitoring the interference dip shift under a broadband light source. If a single-wavelength laser is employed as the light source, the lateral stress variation would manifest as a change in the output light intensity as shown in Fig. 4(a). For optimal performance, the laser wavelength should align with the wavelength of the spectrum's Q points. Q points are the points with the highest slope in the spectrum. Firstly, setting the wavelength range from 1540 nm to 1560 nm, and the resolution is 0.02 nm. Then, exporting the spectrum to the data processing software to get the first-order derivative to find the maximum value. Finally, input the corresponding wavelength to the tunable single-wavelength laser for the following process. If the input lateral stress change is a periodical signal, the following output light intensity change is also a periodical signal with the same frequency. Then, a PD can be used for demodulating the light intensity change, outputting an electrical signal, of which the frequency is the same as the original input HR and RR signals. Thus, the proposed SI structure can be used for vital signs monitoring.

As shown in Fig. 4(b), a section of the SI is struck between two acrylic plates and then put under the body of a still-lying person. People's heartbeat and breath introduce a periodical lateral stress fluctuation on the sensor. Using this sensor and a PD, the heartbeat and breath signal can be transferred into an electrical signal, which is more easily analyzed and recorded. The HR signal recorded by this method is a ballistic force signal generated by the heart, referred to as a ballistocardiograph (BCG). The electrocardiography (ECG) signal is recorded simultaneously to verify the usability of the proposed sensor, as shown in Fig. 4(c). ECG signals are obtained by three patches placed on the chest and abdomen.

In this study, we recruited 5 healthy subjects and one subject with PAC. All subjects signed informed consent. Their ECG and BCG were measured simultaneously.

A. Respiratory Rate and Heart Rate

Fig. 5 shows the experimental results of one subject. The red line is the ECG signal, which has obvious heartbeat peaks. The blue line is the raw data obtained from the PD. There are several peaks, one by one corresponding to the ECG heartbeat signal. Filtered by a low-frequency filter, the breath signal is obtained and marked as a purple line. The experimenter's breathing frequency is about 13 breaths per minute, in the normal range of the human RR.

Because the frequency of the heartbeat signal is around 1 Hz, a band-pass frequency filter is used to extract the heartbeat signal. The result is shown in Fig. 5 by a green line. The proposed sensor recovers the heartbeat signal in detail. The HR is about 63 beats per minute. There is a time delay between the BCG and ECG signals. The reason for this phenomenon is that the monitoring mechanisms for the two signals are entirely different. The ECG signal is obtained by monitoring the electrical signal during the heartbeat.

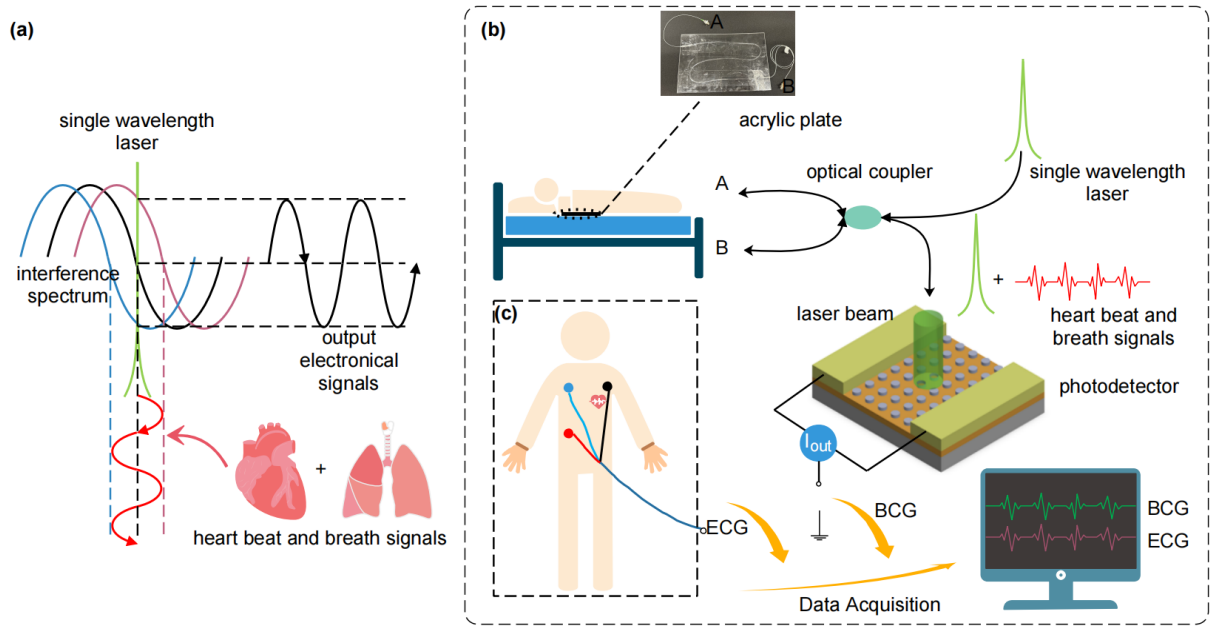

Fig. 4. (a) The principal diagram of light intensity demodulation; (b)The vital signs monitoring sensor; (c) The data acquisition position of the ECG signal.

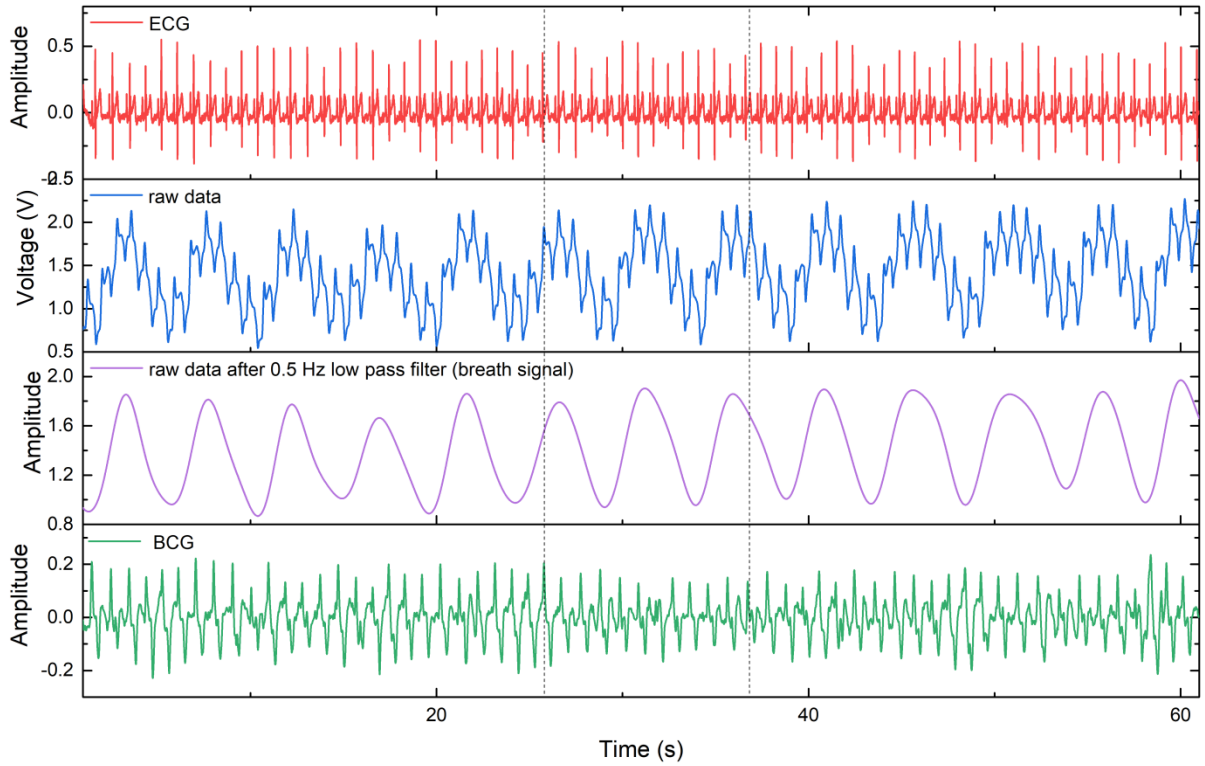

Fig. 5. 60 seconds of ECG, original electrical signal, breath signal, and demodulated BCG signal acquired from one healthy subject.

The BCG signal is obtained by tracking the body vibration caused by the heartbeat [18-19].

To verify the accuracy of the BCG signal obtained and explore the correlation between BCG and ECG signal, a Bland-Altman analysis was performed on the adjacent RR interval of ECG and JJ interval of BCG [20-21]. R wave is the most obvious part of the ECG signal, while J wave is the highest amplitude wave in the BCG signal [22-24]. The results show that the JJ interval obtained by the proposed sensor is highly correlated with the RR interval obtained by the standard ECG monitor, with Pearson's R equal to 0.9984. Fig. 6 shows the Bland-Altman results of the 95% limits of agreement (LOA) for these two parameters. The vast majority of data points are included in the 95% LOA, indicating that the consistency between the RR interval and the JJ interval is high enough. Thus, the proposed sensing system can replace the traditional ECG system to monitor HR.

B. Cardiac Premature Beat

PAC refers to an abnormal electrical impulse from the atrium outside the sinoatrial node of the heart, which causes a

premature atrial contraction [25]. Although isolated premature atrial beats are usually harmless and may occur occasionally in healthy people, frequent premature atrial beats may be a sign of potential cardiovascular problems. They may even cause more serious arrhythmias, such as atrial fibrillation [26]. Therefore, accurate identification and monitoring of premature atrial beats are clinically significant. Fig. 7 shows the heartbeat waveform of a subject with PAC. The subject had two abnormal heartbeats in 30 seconds, marked with a blue background. Both ECG and BCG signals can clearly show abnormal heartbeats. This study's results show that the proposed sensor can accurately capture the abnormal heartbeat signal and can be used as a potential application to help PAC patients monitor their heart health.

Poincaré plot is a graphical tool to visualize and quantify the variability and correlation between consecutive data points in a time series, especially used to analyze the Heart Rate Variability (HRV) Thus, in this experiment, Poincaré plots of the 5 healthy subjects and 1 subject with PAC are drawn to verify whether the proposed sensing system has identification error between healthy subjects and subjects with PAC.

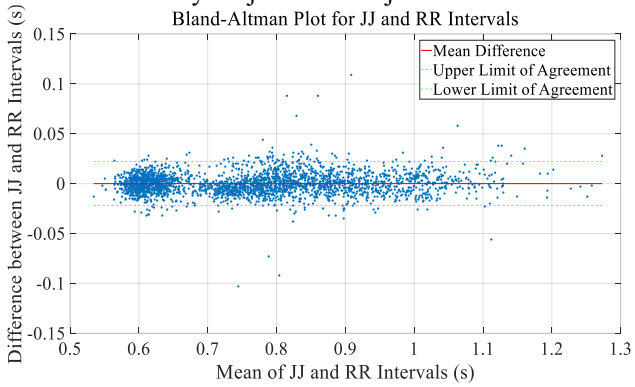

Fig. 6 Bland-Altman analysis result.

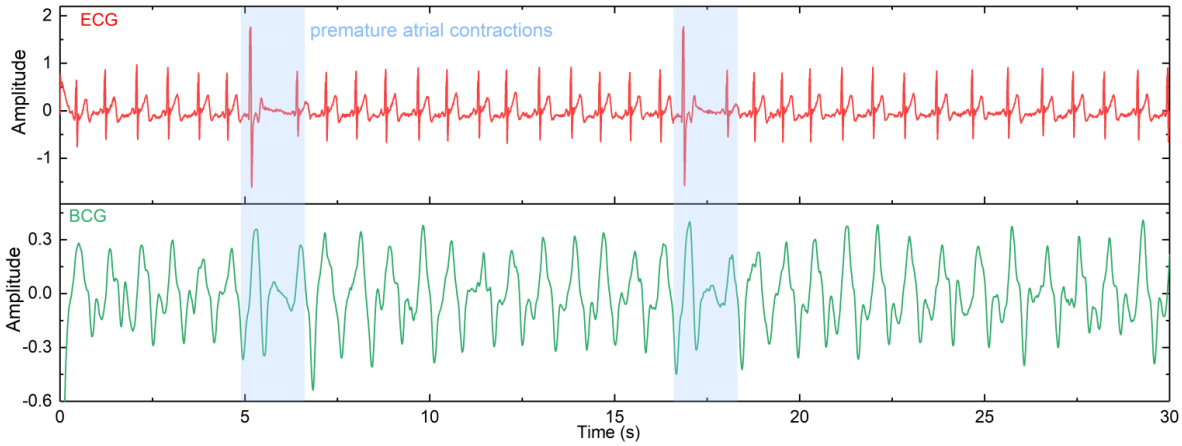

Fig. 7 ECG and BCG signals of a subject with PAC.

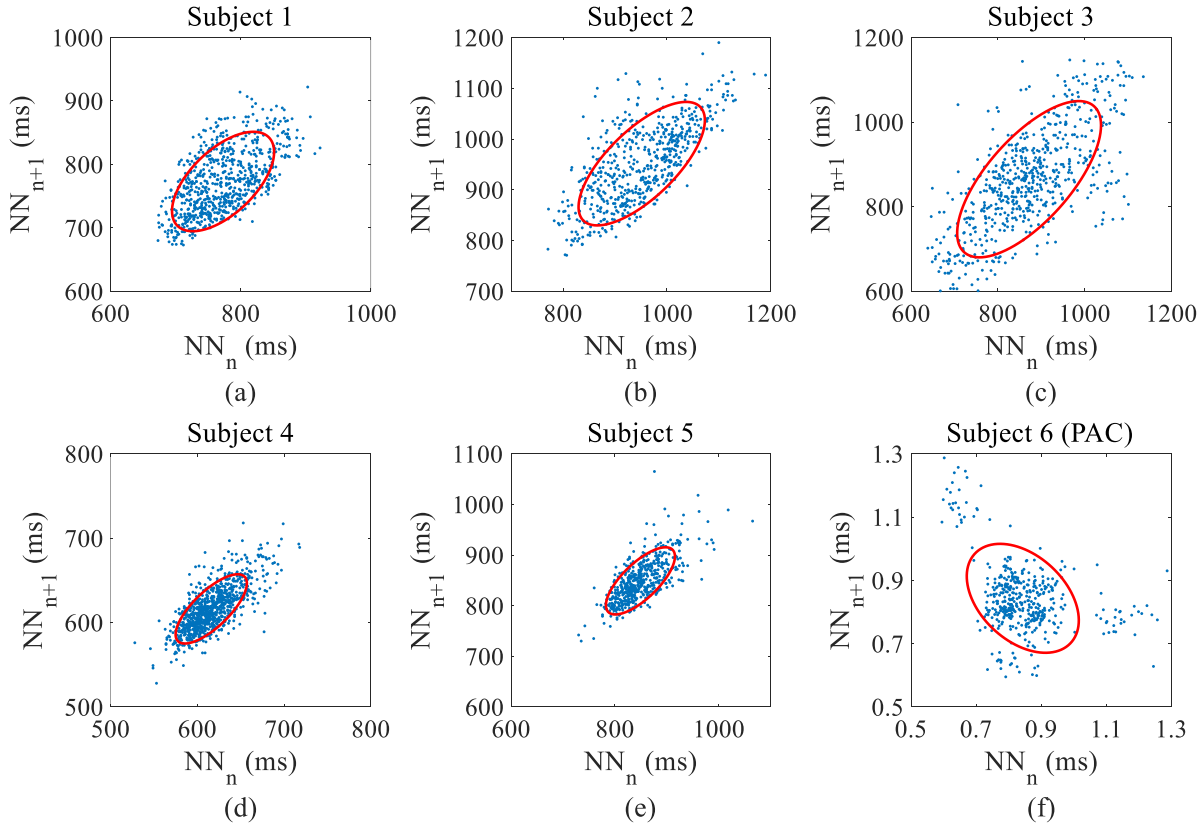

Fig. 8. (a) to (e) The Poincaré plots of the 5 healthy subjects, (f) the Poincaré plot of the subject with PAC.

Fig. 8 (a) to (e) shows the Poincaré plots of the collected BCG signals from 5 healthy subjects, while Fig. 8 (f) shows the Poincaré plots of the collected BCG signal from subjects with PAC. The ellipses in the Poincaré plot of healthy people are usually tilted, and the ratio of their major and minor axes reflects HRV. The Poincaré plot of healthy people rarely shows obvious discrete points. The plot often shows a relatively compact and symmetrical ellipse or similar shape, indicating normal HRV and stable heartbeat patterns. The Poincaré plot of patients with premature beats may show more complex structures, including multiple small ellipses or other atypical shapes, because premature beats disrupt the originally smooth heartbeat sequence. The plot may show additional discrete points or abnormal clusters, which are located outside the main ellipse and represent sudden changes in heartbeat intervals caused by premature beats. Premature beats introduce significant discrete points that are discontinuous with the main distribution because the JJ interval caused by premature beats is significantly shorter than the normal sinus JJ interval, and the subsequent compensatory pause makes the next JJ interval longer. Thus, this method helps assess the heartbeat situation of one person based on the BCG data collected by the proposed sensor.

C. Sensing Performance analysis

Compared with other fiber-based vital signs monitoring sensors, the proposed sensor demonstrates clear advantages across multiple dimensions, as shown in Table I. It exhibits low sensitivity to ambient temperature, low cost, and a simple manufacturing process, making it a highly efficient and practical choice. Additionally, it achieves high BCG signal quality, which is sufficient to enable PAC detection, a critical feature for early cardiovascular monitoring. In contrast, while traditional sensors like FBG and POF (polymer optical fiber) offer moderate to high sensitivity and complexity, they come with higher costs and lower BCG quality. The bending loss sensor, though cost-effective and temperature-stable, falls short in BCG performance and manufacturing simplicity. Overall, the proposed sensor offers a well-balanced and superior design for practical applications.

TABLE I
SENSING PERFORMANCE COMPARISON WITH OTHER FIBER-BASED STRUCTURES

Sensing Structure	Temperature Sensitivity	Cost	Fabrication Process Complexity	BCG quality	Ref
Proposed sensor	-	Low	Simple	High	
Bending loss	Low	Low	Complex	Low	[27]
FBG	Medium	High	Complex	Medium	[28]
POF	Medium	High	Complex	Low	[29]

V. CONCLUSION

In this paper, an optical non-invasive vital signs monitoring sensor was established, and the effectiveness of the sensor was demonstrated. The core part of the sensor is a fiber SI, which consists of a 3 dB coupler and a section of homemade SH-HiBiF. This SI structure can measure the external lateral stress change based on demodulating the interference dip shift. Even without contact with the human body, the proposed monitoring sensor can also monitor breath and heartbeat rates based on demodulating the light intensity change. The heart signal collected by the proposed sensor has a consistency of up to 95% with the data collected by traditional electrical sensors. In addition, this sensor can accurately capture the abnormal heartbeat signal to help assess the cardiac health status of PAC patients. This study illustrates the feasibility of the proposed sensor for further research in the biomedical field.

REFERENCE

[1] Hoang ChuDuc, Kien NguyenPhan, Dung NguyenViet, "A Review of Heart Rate Variability and its Applications," APCBEE Procedia, vol.7, pp. 80-85, 2013.
[2] Acharya U, R., N, K., Sing, O.W. et al., "Heart rate analysis in normal subjects of various age groups." Biomedical Engineering Online, vol. 3, art. no. 24, July 2004.
[3] Heikki V. Huikuri, Timo H. Mäkikallio, "Heart rate variability in ischemic heart disease", Autonomic Neuroscience, vol. 90, no. 1–2, pp. 95-101, July 2001.
[4] S. Boonnithi and S. Phongsuphap, "Comparison of heart rate variability measures for mental stress detection", 2011 Computing in Cardiology, Hangzhou, China, pp. 85-88, 2011.
[5] Nogués, Martín A. MD, Benarroch, Eduardo MD., "Abnormalities of Respiratory Control and the Respiratory Motor Unit", The Neurologist, vol. 14, no. 5, pp. 273-288, Sept. 2008.
[6] N. Giardino, P. Lehrer, and R. Edelberg, "Comparison of finger plethysmograph to ECG in the measurement of heart rate variability," Psychophysiology, vol. 39, no. 2, pp. 246–253, 2002.
[7] D. Biswas, N. Simoes-Capela, C. Van Hoof, and N. Van Helleputte, "Heart rate estimation from wrist-worn photoplethysmography: a review," IEEE Sensors Journal, vol. 19, no. 16, pp. 6560–6570, 2019.
[8] C. L. Levkov, "Orthogonal electrocardiogram derived from the limb and chest electrodes of the conventional 12-lead system," Medical & Biological Engineering & Computing, vol. 25, no. 2, pp. 155–164, 1987.
[9] C. Massaroni et al., "Validation of a wearable device and an algorithm for respiratory monitoring during exercise", IEEE Sens. J., vol. 19, no. 12, pp. 4652–4659, 2019.
[10] A. Ukil, H. Braendle and P. Krippner, "Distributed temperature sensing: Review of technology and applications", IEEE Sensors Journal, vol. 12, no. 5, pp. 885-892, May 2012.
[11] Z. Chen et al., "Simultaneous measurement of breathing rate and heart rate using a micro-bend multimode fiber optic sensor," Journal of Biomedical Optics, vol. 19, no. 5, pp. 057001, May. 2014.

[12] C. Massaroni et al., "Design and Feasibility Assessment of a Magnetic Resonance-Compatible Smart Textile Based on Fiber Bragg Grating Sensors for Respiratory Monitoring," IEEE Sensors Journal, vol. 16, no. 22, pp. 8103-8110, Nov.15, 2016.
[13] Z. Chen et al., "Simultaneous measurement of breathing rate and heart rate using a micro-bend multimode fiber optic sensor," Journal of Biomedical Optics, vol. 19, no. 5, pp. 057001, May. 2014.
[14] C. Massaroni et al., "Design and Feasibility Assessment of a Magnetic Resonance-Compatible Smart Textile Based on Fiber Bragg Grating Sensors for Respiratory Monitoring," IEEE Sensors Journal, vol. 16, no. 22, pp. 8103-8110, Nov.15, 2016.
[15] Fengze Tan, Shuyang Chen, Weimin Lyu, Zhengyong Liu, Changyuan Yu, Chao Lu, and Hwa-Yaw Tam, "Non-invasive human vital signs monitoring based on twin-core optical fiber sensors," Biomedical Optics Express, vol. 10, no. 11, pp. 5940-5952, Oct. 2019.
[16] Weihao Yuan, Lingduo Li, Yu Wang, Zhenggang Lian, Daru Chen, Changyuan Yu, and Chao Lu, "Temperature and curvature insensitive all-fiber sensor used for human breath monitoring," Optics Express, vol. 29, no. 17, pp. 26375-26384, Aug. 2021.
[17] Z. Liu, C. Wu, M. L. V. Tse and H. Y. Tam, "Fabrication, Characterization, and Sensing Applications of a High-Birefringence Suspended-Core Fiber," *Journal of Lightwave Technology*, vol. 32, no. 11, pp. 2113-2122, June, 2014.
[18] P. K. Jain and A. K. Tiwari, "Heart monitoring sensors—A review," Computers in Biology and Medicine, vol. 54, pp. 1–13, 2014, doi: 10.1016/j.compbiomed.2014.08.014.
[19] Starr I, Verdouw PD, Noordergraaf A. "Clinical evidence of cardiac weakness and incoordination secured by simultaneous records of the force BCG and carotid pulse derivative and interpreted by an electrical analogue," American Heart Journal, vol. 85, no.3, pp. 341-8, 1973.
[20] J. E. Barnhill, M. Tendera, H. Cade, W. B. Campbell, and R. F. Smith, "Depolarization changes early in the course of myocardial infarction: Significance of changes in the terminal portion of the QRS complex," Journal of the American College of Cardiology, vol. 14, no. 1, pp. 143–149, 1989, doi: 10.1016/0735-1097(89)90064-8.
[21] J. H. Shin, B. H. Choi, Y. G. Lim, D. U. Jeong, and K. S. Park, "Automatic ballistocardiogram (BCG) beat detection using a template matching approach," 2008 30TH Annual International Conference of the IEEE Engineering in Medicine and Biology Society, vol. 1-8, pp. 1144–1146, 2008, doi: 10.1109/IEMBS.2008.4649363.
[22] W. Lyu et al., "Non-Contact Short-Term Heart Rate Variability Analysis Under Paced Respiration Based on a Robust Fiber Optic Sensor," IEEE Transactions on Instrumentation and Measurement, vol. 73, pp. 1–13, 2024, doi: 10.1109/TIM.2023.3346511.
[23] R. Casanella, J. Gomez-Clapers, and R. Pallas-Areny, "On time interval measurements using BCG," in 2012 Annual International Conference of the IEEE Engineering in Medicine and Biology Society, IEEE, 2012, pp. 5034–5037. doi: 10.1109/EMBC.2012.6347124.
[24] D. D. He, E. S. Winokur, and C. G. Sodini, "An ear-worn continuous ballistocardiogram (BCG) sensor for cardiovascular monitoring," 2012 Annual International Conference of the IEEE Engineering in Medicine and Biology Society, pp. 5030–5033, 2012, doi: 10.1109/EMBC.2012.6347123.
[25] C. Y. Guo, K. J. Wang, and T. L. Hsieh, "Piezoelectric sensor for the monitoring of arterial pulse wave: Detection of arrhythmia occurring in pac/pvc patients," Sensors (Basel, Switzerland), vol. 21, no. 20, pp. 6915-, 2021, doi: 10.3390/s21206915.
[26] J. B. Guichard, E. Guasch, F. Roche, A. Da Costa, and L. Mont, "Premature atrial contractions: A predictor of atrial fibrillation and a relevant marker of atrial cardiomyopathy," Frontiers in Physiology, vol. 13, pp. 971691-, 2022, doi: 10.3389/fphys.2022.971691.
[27] R. Zhao *et al.*, "Accurate Estimation of Heart and Respiration Rates Based on an Optical Fiber Sensor Using Adaptive Regulations and Statistical Classifications Spectrum Analysis," *Frontiers in digital health*, vol. 3, pp. 747460–747460, 2021.
[28] L. Zhichao, Z. Xi, S. Taoping, and M. Jiahe, "Heartbeat and respiration monitoring based on FBG sensor network," *Optical fiber technology*, vol. 81, pp. 103561, 2023.
[29] L. Li, C. Yang, Z. Wang, K. Xiao, and R. Min, "Stretchable polymer optical fiber embedded in the mattress for respiratory and heart rate monitoring," *Optics and laser technology*, vol. 171, pp. 110356, 2024.